Extended Abstract

Synthesizing Ytterbium-Substituted ($Y_3Yb_xFe_{5-x}O_{12}$) Nanostructures by the Sol–Gel Method and Investigating Their Structural and Electromagnetic Properties.

Seyed Ebrahim Mousavi Ghahfarokhi[1, 2, *], Amin Esmailvandi[1]

[1]Department of Physics, Faculty of Science, Shahid Chamran University of Ahvaz, Ahvaz, Iran

[2]Center for Research on Laser and Plasma, Shahid Chamran University of Ahvaz, Ahvaz, Iran,

Received: 03.11.2025 Final revised: 27.10.2025 Accepted: 30.11.2025 Published On-Line: 31.12.2025

DOI: 10.22055/jrmbs.2025.20484

Introduction

Yttrium iron garnet (YIG) is considered one of the most important ferrimagnetic compounds, owing to its highly ordered crystal structure and exceptional magnetic properties. These characteristics have attracted extensive attention across a wide range of scientific and industrial applications. The material, commonly referred to by its abbreviation YIG, exhibits features such as high electrical resistivity, high magnetic permeability, low energy loss, and good thermal stability. Such properties have enabled its utilization in diverse fields, including microwave technology, wireless communication systems, optoelectronics, and data storage. YIG possesses a body-centered cubic (bcc) crystal structure and belongs to the space group $Ia_3d\ O_h^{10}$. Each conventional unit cell of this compound contains eight formula units with the chemical composition $Y_3Fe_5O_{12}$. The cation distribution is represented as $\{Y_3^{3+}\}_c\left[Fe_2^{3+}\right]_a\left(Fe_3^{3+}\right)_d$, where a, c, and d correspond to octahedral, dodecahedral, and tetrahedral sites, respectively. In this structure, there are 24 dodecahedral, 16 octahedral, and 24 tetrahedral sites, with yttrium ions occupying the dodecahedral sites and iron ions occupying the octahedral and tetrahedral sites. In recent years, substituted yttrium iron garnet nanoparticles doped with various elements have garnered considerable scientific interest due to their distinctive magnetic, optical, and electronic properties, as well as their broad technological potential. By substituting cations with different ionic radii or magnetic characteristics, it becomes possible to tailor and enhance the material's functionalities [1-3]. According to available studies, no report has been presented so far on the substitution of ytterbium ions in the yttrium iron garnet structure or on an investigation of its

* Corresponding Author: Musavi_ebrahim@yahoo.co.uk

This work is licensed under a Creative Commons Attribution 4.0 International License

structural and electromagnetic properties. Therefore, the present study focuses on examining the effects of ytterbium ion substitution on the structural, magnetic, and dielectric properties of yttrium iron garnet.

Experimental procedures

In this study, the sol–gel method was employed to synthesize substituted yttrium iron garnet nanostructures, Y3YbxFe5-xO12, with substitution values (x = 0, 0.1, 0.2, 0.5, 1.0, 2.0, 2.5, 3.0). For this purpose, the starting materials, including iron nitrate Fe $(NO_3)_3 \cdot 9H_2O$, yttrium nitrate $Y(NO_3)_3 \cdot 6H_2O$, and ytterbium chloride $YbCl_3 \cdot 6H_2O$, were dissolved in 25 mL of deionized water. Then citric acid was added to the solution for complexation. In the next step, an ammonia solution was used to adjust the pH to pH = 2. The resulting gel, after the aging process, was placed in an electric oven at 115 °C for 48 hours to dry, and in the final step, the dried gel was calcined in an electric furnace at 900 °C for 2 hours.

Characterization Methods

Phase identification and the crystal structure of the samples were studied by X-ray diffraction (XRD), and the chemical bonds of the samples were investigated by Fourier-transform infrared spectroscopy (FT-IR) over the wavenumber range 400–4000 cm^{-1}. The microstructure of the samples was examined by field emission scanning electron microscopy (FE-SEM). The magnetic hysteresis curves of the samples were measured by a vibrating sample magnetometer (VSM) over the range -15000 to +15000 Oe. Also, to investigate dielectric properties, permeability, and magnetic loss of yttrium-iron garnet, an LCR meter was used.

Structural Results

Figure (1) presents the X-ray diffraction (XRD) patterns of ytterbium-substituted yttrium iron garnet powders, $Y_3Yb_XFe_{5-X}O_{12}$, with substitution levels of x = 0, 0.1, 0.15, 0.2, 0.25, and 0.3. According to the XRD patterns, the diffraction profiles of the samples are consistent with the standard card (01-071-2150) corresponding to $Y_3Fe_5O_{12}$, indicating the formation of a single-phase cubic garnet structure in all compositions. However, in the sample with x = 0.3, an additional peak associated with $YbFeO_3$ appears at the position $2\theta = 33.47°$, in agreement with

the standard card (01-074-1482). Based on the XRD data, the gradual increase in Yb^{3+} concentration causes the diffraction peaks to shift toward lower angles, reflecting an increase in the lattice constant. The lattice parameter increases from 12.26 Å in the unsubstituted sample to 12.32 Å for x = 0.3. This expansion can be attributed to the substitution of Yb^{3+} ions with a larger ionic radius (0.86 Å) in place of Fe^{3+} ions (0.68 Å), which leads to an enlargement of the unit cell volume [4,5]. Furthermore, the crystallite size was estimated to be in the range of 30–36 nm. At a low substitution amount of x = 0.1, an increase in crystallite size is observed, which can be ascribed to the reduction of lattice strain. However, at x = 0.3, the crystallite size decreases to approximately 30 nm, likely due to enhanced crystal strain and the onset of secondary phase formation $YbFeO_3$ [6]. The theoretical density of the samples shows an increasing trend with higher Yb^{3+} content, resulting from the replacement of the heavier Yb^{3+} ion (173 g/mol) for Fe^{3+} (55.58 g/mol). Despite the expansion of the lattice parameter, the theoretical density increases from 5.31 g/cm³ for the base sample to 5.49 g/cm³ at x = 0.3, indicating that the effect of molar mass predominates over the volume expansion of the unit cell. Overall, it can be concluded that controlled substitution of Yb^{3+} ions up to x = 0.25 promotes lattice expansion without damaging the garnet phase. However, higher substitution levels beyond this threshold lead to disruption in crystallite growth, increased structural strain, and the formation of secondary phases, which directly influence the magnetic and electrical properties of the system. The detailed XRD pattern information for the samples is summarized in Table 1.

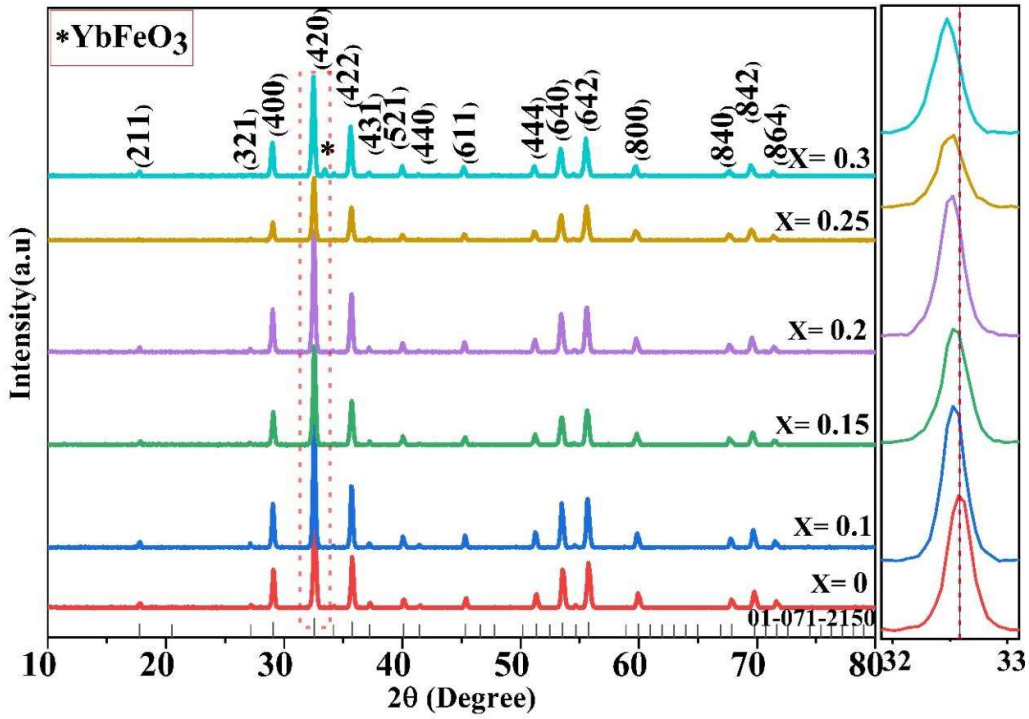


Figure 1: X-ray diffraction pattern of samples substituted with ytterbium ion $Y_3Yb_xFe_{5-x}O_{12}$ with values of x = 0, 0.1, 0.15, 0.2, 0.25, and 0.3.

Table 1: Phase percentage, nanocrystal size, lattice constant, lattice strain, unit cell volume, and X-ray density of ytterbium ion-substituted samples $Y_3Yb_xFe_{5-x}O_{12}$.

theoretical density g/cm³	volume of the unit cell Å³	lattice strain $\varepsilon\times10^{-3}$	lattice parameter a Å	crystallite size D(nm)	Phase percentage	substitution levels (x)
5.31	1842.77	3.80	12.26	34	100%	0
5.35	1859.5	3.47	12.30	36	100%	0.1
5.40	1856.33	3.71	12.29	34	100%	0.15
5.43	1860.86	3.62	12.30	35	100%	0.2
5.32	1851.80	3.64	12.28	35	100%	0.25
5.49	1869.95	4.19	12.32	30	97%	0.3

Figure (2) illustrates the Fourier-transform infrared (FT-IR) spectra of ytterbium-substituted yttrium iron garnet samples.

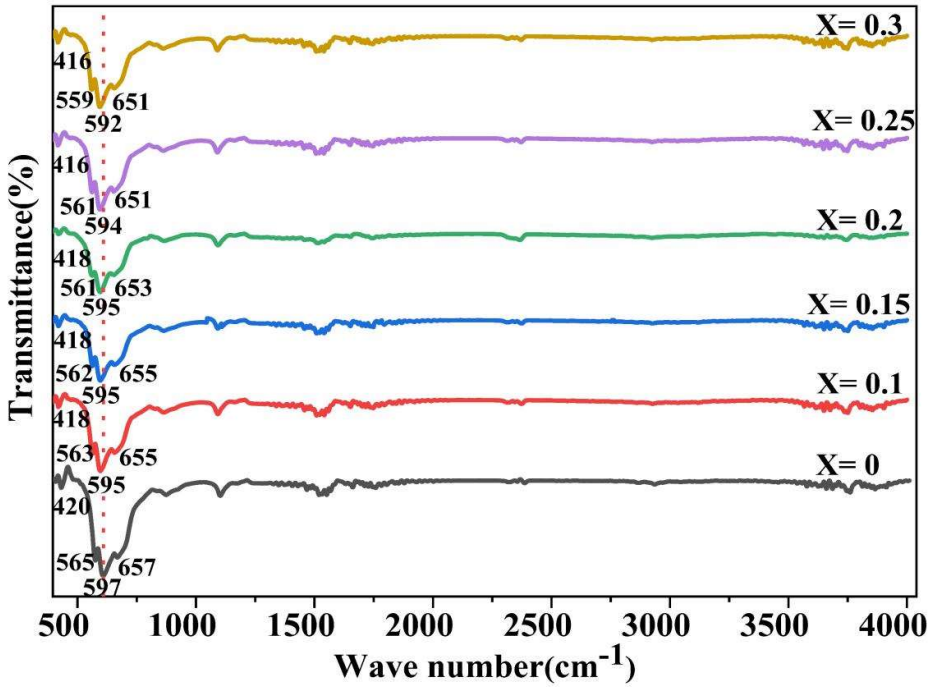


Figure 2: FT-IR spectra of samples substituted with ytterbium ion $Y_3Yb_xFe_{5-x}O_{12}$ with values of x = 0, 0.1, 0.15, 0.2, 0.25, and 0.3.

According to previous reports [7], seventeen infrared-active vibrational modes are present in the garnet structure. These include three asymmetric stretching modes at tetrahedral sites (ν_3), three asymmetric bending modes (ν_4), one symmetric bending mode (ν_2), two rotational modes R related to tetrahedral positions, two translational modes (T) corresponding to tetrahedral sites, three translational modes (T_d) associated with cations in dodecahedral sites, and three translational modes (T_0) arising from cations located in octahedral sites. In this study, the three stretching modes recorded in the range of 550–660 cm^{-1} were assigned to oxygen–metal bond stretching vibrations at tetrahedral sites (ν_3). Similarly, the modes observed within 416–420 cm^{-1} were attributed to oxygen–metal bending vibrations at octahedral sites (ν_4) [7]. With increasing substitution of Yb^{3+} ions in place of Fe^{3+}, the main absorption peaks exhibit a noticeable shift toward lower wavenumbers. This shift results from the larger ionic radius of Yb^{3+} relative to Fe^{3+}, which leads to an elongation of the Fe–O bond length within the lattice and a consequent reduction in vibrational energy. Therefore, lower vibrational frequencies are detected, manifested as peak displacements toward smaller wavenumbers in the spectrum. These spectral changes provide clear evidence of successful incorporation of ytterbium ions and the influence of their substitution on the bonding characteristics within the yttrium iron garnet lattice [4].

Morphology

Figure 3 shows the FE-SEM image of the synthesized samples. FE-SEM images demonstrated that the morphology of the samples changed with substitution, transforming from an almost spherical state in the pure sample to coral-like structures in the substituted samples [4].

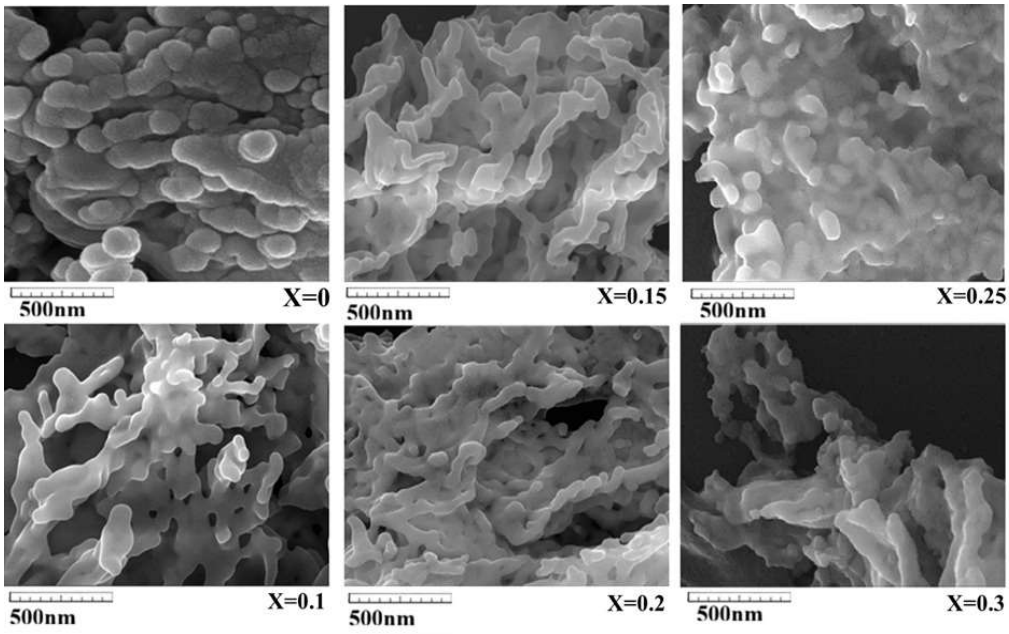


Figure 3: FE-SEM images of ytterbium ion-substituted samples $Y_3Yb_xFe_{5-x}O12$ with values of x = 0, 0.1, 0.15, 0.2, 0.25, and 0.3.

Magnetic Results

Figure 4 presents the magnetic hysteresis curves of the ytterbium-substituted yttrium iron garnet (YIG) samples. According to the magnetic hysteresis plots, the variation of saturation magnetization (Ms) in the substituted samples with the general formula $Y_3Yb_xFe_{5-x}O_{12}$ exhibits a nonlinear trend. Considering that the ionic radius of Yb^{3+} is larger than that of Fe^{3+}, the probability of Yb^{3+} occupying octahedral sites is greater than that of tetrahedral sites. At the initial substitution level x = 0.1, the saturation magnetization of the Yb-substituted sample decreases compared to that of the pure YIG sample. This decrease can be attributed to spin canting at the tetrahedral sites caused by the presence of Yb^{3+} ions in the octahedral positions [8]. With increasing substitution up to x = 0.2, the saturation magnetization gradually increases and reaches a maximum value of 28.3 emu/g. The observed trend in the variation of saturation magnetization in this work is

consistent with the results reported by García et al. [4]. Given that Yb^{3+} ions have a smaller magnetic moment (4.3–4.9 μB) than Fe^{3+} ions (5 μB), this increase can be ascribed to the dominant influence of the reduction in magnetic moment arising from Yb^{3+} substitution at octahedral sites over the decrease caused by spin canting [8, 9]. For higher substitution levels ($x \geq 0.25$), the saturation magnetization starts to decrease. This reduction can be attributed to modifications in the superexchange interactions between Fe ions (Fe_d–O–Fe_a) due to the presence of Yb^{3+} ions, as well as to the appearance of the $YbFeO_3$ impurity phase detected in the sample with $x = 0.3$ [8]. As the substitution level of Yb^{3+} ions replacing Fe^{3+} increases, the coercivity (Hc) exhibits a decreasing trend, indicating an improvement in the soft magnetic behavior of the YIG samples. The incorporation of Yb^{3+} ions—which possess smaller magnetic moments and weaker magnetic properties compared to Fe^{3+} ions—leads to a reduction in the magnetocrystalline anisotropy constant (K). Since coercivity (Hc) is directly proportional to K, the decrease in anisotropy results in lower coercivity values [10]. The squareness ratio (Mr/Ms) of all samples is less than 0.5, indicating that the samples possess multi-domain magnetic structures [10]. The magnetic parameters obtained from the hysteresis loops are summarized in Table 2. Figure (5) shows the magnetic susceptibility (χ) as a function of the applied magnetic field (H), determined using the relation ($\chi = dM/dH$). Based on the data in Table 2, the magnetic susceptibility of the samples increases with the amount of Yb^{3+} substitution. As illustrated in Figure 5, the susceptibility curve exhibits a single peak for all samples except for $x = 0.3$, where two relative peaks are observed, indicating the presence of an impurity phase in this sample. This observation is consistent with the results obtained from the X-ray diffraction patterns.

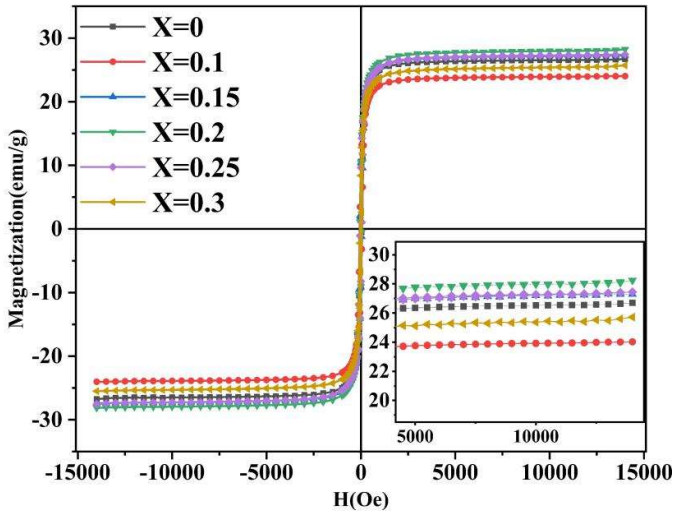


Figure 4: Hysteresis diagram of ytterbium ion-substituted samples $Y_3Yb_xFe_{5-x}O12$ with values of x = 0, 0.1, 0.15, 0.2, 0.25, and 0.3.

Table 2: Magnetic properties of samples substituted with ytterbium ions $Y_3Yb_xFe_{5-x}O_{12}$.

K (emu/g.Oe)	χ	Mr/Ms	H_c (Oe)	Mr (emu/g)	Ms (emu/g)	substitution levels (x)
1474	0.210	0.396	53	10.5	26.7	0
1651	0.169	0.422	66	10.1	24	0.1
1621	0.199	0.380	57	10.4	27.3	0.15
1559	0.208	0.370	53	10.5	28.3	0.2
1294	0.215	0.350	44	9.6	27.5	0.25
963	0.201	0.326	36	8.4	25.7	0.3

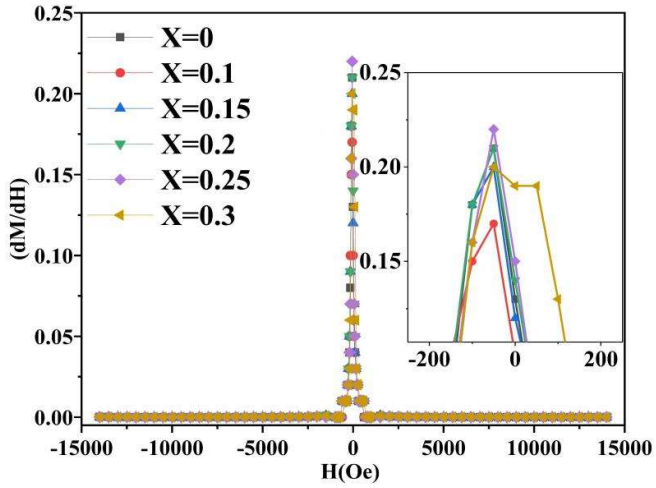


Figure 5: Magnetic susceptibility of ytterbium ion-substituted samples $Y_3Yb_xFe_{5-x}O_{12}$ with values of x = 0, 0.1, 0.15, 0.2, 0.25, and 0.3.

Electromagnetic Results

Figures 6, 7, and 8 show the dielectric constant (ε′), dielectric loss (ε″), and AC electrical conductivity (σ_{ac}) as a function of frequency, respectively. LCR meter results showed that the dielectric constant (ε′) and dielectric loss (ε″) of the samples decreased, while the AC electrical conductivity (σ_{ac}) increased with increasing frequency. This behavior was explained by the surface polarization model and the Maxwell-Wagner–Koops theory. Furthermore, at a specific frequency, increasing the amount of Yb^{3+} caused all three components (ε′, ε″, and σ_{ac}) to decrease. This phenomenon is due to the reduced electron hopping ability between Fe^{2+} and Fe^{3+} ions, resulting from a decrease in the concentration of iron ions at the octahedral sites due to the presence of the Yb^{3+} ion [11].

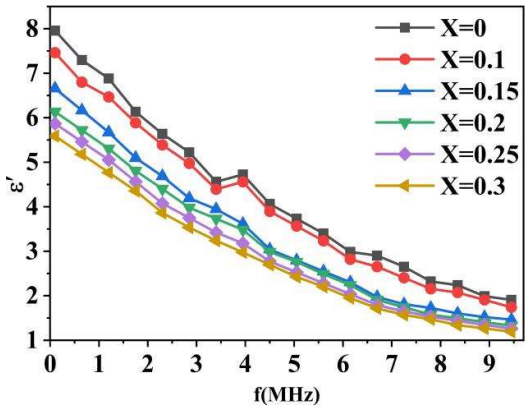


Figure 6: dielectric constant of ytterbium ion-substituted samples $Y_3Yb_xFe_{5-x}O_{12}$ with values of x = 0, 0.1, 0.15, 0.2, 0.25, and 0.3.

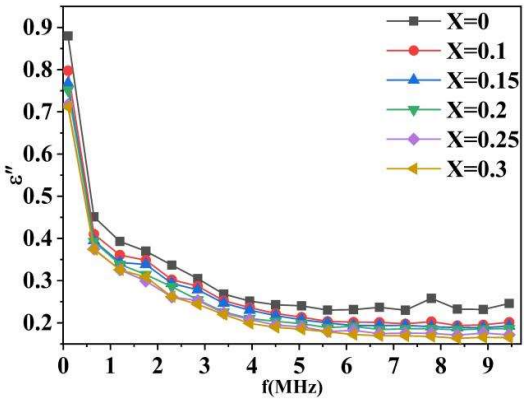


Figure 7: dielectric loss of ytterbium ion-substituted samples $Y_3Yb_xFe_{5-x}O_{12}$ with values of x = 0, 0.1, 0.15, 0.2, 0.25, and 0.3.

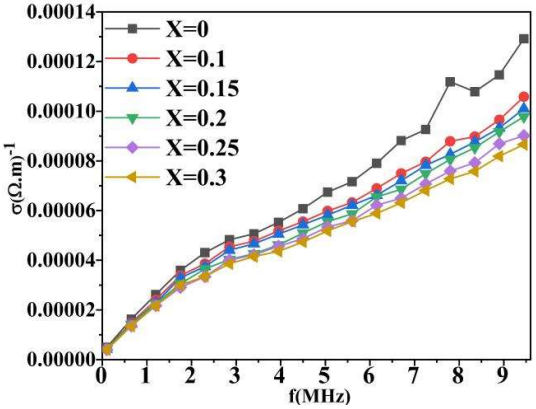


Figure 8: AC electrical conductivity of ytterbium ion-substituted samples $Y_3Yb_xFe_{5-x}O_{12}$ with values of x = 0, 0.1, 0.15, 0.2, 0.25, and 0.3.

Figures 9 and 10 present the magnetic permeability (μ′) and magnetic loss (μ″) of the samples, respectively. The permeability (μ′) and magnetic loss (μ″) of the samples decreased with increasing frequency, which is a natural behavior for ferrites attributed to the restriction of domain wall movement with increasing frequency [12].

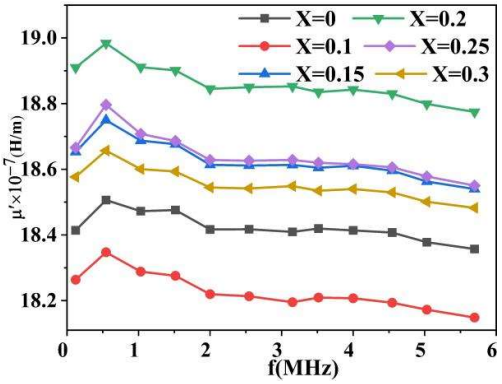


Figure 9: magnetic permeability of ytterbium ion-substituted samples $Y_3Yb_xFe_{5-x}O_{12}$ with values of x = 0, 0.1, 0.15, 0.2, 0.25, and 0.3.

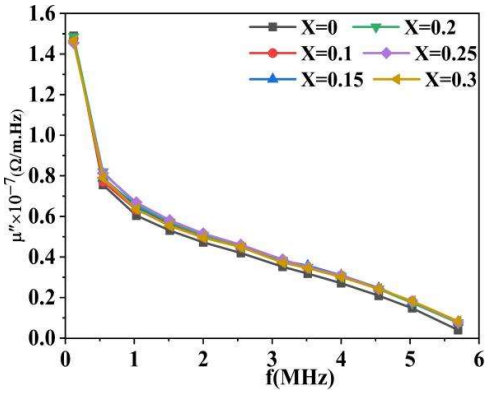


Figure 10: magnetic loss of ytterbium ion-substituted samples $Y_3Yb_xFe_{5-x}O_{12}$ with values of x = 0, 0.1, 0.15, 0.2, 0.25, and 0.3.

Conclusion

XRD results confirmed the single-phase garnet structure for samples with x≤0.25 and the presence of the impurity phase $YbFeO_3$ for the x=0.3 sample. The lattice constant increased with increasing substitution, which is due to bond stretching caused by the substitution of the ytterbium ion, which has a larger ionic radius than the iron ion. The crystallite size varied in the range of 30 to 36 nm, consistent with the effect of lattice strain. The saturation magnetization increased from 26.7 emu/g in the x=0 sample to a maximum value of 28.3 emu/g in the x=0.2 sample and then decreased with further increase in Ytterbium content. The coercivity decreased from 53 Oe to 36 Oe, indicating an improvement in the soft magnetic behavior of the samples with increased substitution. The investigation of electromagnetic properties also showed that the dielectric constant, dielectric loss, and AC conductivity decrease with increasing substitution. This behavior was attributed to the reduced concentration of exchangeable Fe^{3+} and Fe^{2+} ions and the weakening of the interfacial polarization and surface polarization mechanisms. The permeability and

magnetic loss of the samples also decreased with increasing frequency, which is a common behavior for ferrites.

Keywords: Yttrium Iron Garnet (YIG), sol–gel method, Nanostructures, magnetic properties, electrical properties, magnetic permeability.

[1] H. Zheng, et al., Magnetic and dielectric properties of Nd-Sn-Cu co-doped yttrium iron garnet ferrite, Journal of Magnetism and Magnetic Materials, 591 (2024). https://doi.org/10.1016/j.jmmm.2024.171777

[2] M. Niyaifar, A. Behmanesh, A. Hasanpour, An investigation on structural and magnetic properties of praseodymium substituted yttrium iron garnet nanoparticles, Iranian Journal of Crystallography and Mineralogy, 25(2) (2017) 439-448. [In Persian]

[3] O. I. Gorbatov, et al., Magnetic exchange interactions in yttrium iron garnet: A fully relativistic first-principles investigation, PHYSICAL REVIEW B, 104 (2021) 174401. https://doi.org/10.1103/PhysRevB.104.174401

[4] A. Fernández, F. P. Araujo, Y. Guerra, S. Castro-Lopes, J. Matilla-Arias, I. S. de Lima, E. C. Silva-Filho, J. A. Osajima, F. Guerrero, R. Peña-Garcia, Synthesis of coral-like structures of Pr–Yb co-doped YIG: Structural, optical, magnetic and antimicrobial properties, Journal of Rare Earths, 42(3) (2024) 543-554. https://doi.org/10.3390/molecules29020391

[5] T. Ramesh1, J. Naga Vishnu Vardhan, Role of Dysprosium Incorporation on Structural and Magnetic Properties of Yttrium Iron Garnet for High Power Microwave Device Applications," Ceramics International, 51(13) (2025) 18129-18139. https://doi.org/10.1016/j.ceramint.2025.01.588

[6] M. Niayifar, N. Khalafi, A. Hasanpour, Influence of cerium substitution on the microstructure and magnetic properties of yttrium iron garnet, prepared via sol-gel method, Iranian Journal of Crystallography and Mineralogy, 21(2) (2013) 183-190. [In Persian]

[7] A. Pormehr, M. Niyaifar, A. Hassanpour, "Investigation of structural properties of Yttrium Iron Garnet substituted by Antimony fabricated via sol-gel method, Iranian Journal of Crystallography and Mineralogy, 26*(*4) (2019) 1027-1036. [In Persian] doi:10.29252/ijcm.26.4.1027

[8] K. Hamasha, et al., Structural and Magnetic Studies of Ga-doped Yttrium Iron Garnet, Journal of Wuhan University of Technology-Mater, 36(1) (2021) 13-21. https://doi.org/10.1007/s11595-021-2372-3

[9] Y. Jiang, A. Sun, X. Huang, J. Wang, Study on the crystal structure and magnetic properties of Zn-Cu-Co nano ferrite doped with Yb^{3+}, Journal of Alloys and Compounds, 931(1), (2023) 167527. https://doi.org/10.1016/j.jallcom.2022.167527

[10] M. H. El Makdah, M. H. El-Dakdouki, R. Mhanna, J, Al Boukhari, R. Awad, Effects of neodymium substitution on the structural, optical, and magnetic properties of yttrium iron garnet nanoparticles, Applied Physics A, 127(5) (2021) 304. https://doi.org/10.1007/s00339-021-04466-0

[11] N. Rezlescu, E. Rezlescu, Dielectric properties of ferrites in connection with their structure, Physica Status Solidi (A), 23(2) (1974) 575-582. https://doi.org/10.1002/pssa.2210230229

[12] R. Ghamari, Kh. Gheisari, Structure, Microstructure, Magnetic and Electromagnetic Properties Ni-Mn-Zn Ferrite Produced by Glycine-Nitrate Process, journal of New Materials, 7(27) (2017) 45-56. [In Persian] https://dorl.net/dor/20.1001.1.22285946.1396.7.27.4.6